Orientation dependence of structural transition in fcc Al driven under uniaxial compression by atomistic simulations*

Li Li(李 莉)[a], Shao Jian-Li(邵建立)[b], Duan Su-Qing(段素青)[b]†, and Liang Jiu-Qing(梁九卿)[a]

[a] *Institute of Theoretical Physics and Department of Physics, Shanxi University, Taiyuan* 030006, *China*
[b] *Institute of Applied Physics and Computational Mathematics, Beijing* 100088, *China*

(Received 21 July 2010; revised manuscript received 15 November 2010)

By molecular dynamics simulations employing an embedded atom method potential, we have investigated structural transformations in single crystal Al caused by uniaxial strain loading along the [001], [011] and [111] directions. We find that the structural transition is strongly dependent on the crystal orientations. The entire structure phase transition only occurs when loading along the [001] direction, and the increased amplitude of temperature for [001] loading is evidently lower than that for other orientations. The morphology evolutions of the structural transition for [011] and [111] loadings are analysed in detail. The results indicate that only 20% of atoms transit to the hcp phase for [011] and [111] loadings, and the appearance of the hcp phase is due to the partial dislocation moving forward on $\{111\}_{\rm fcc}$ family. For [011] loading, the hcp phase grows to form laminar morphology in four planes, which belong to the $\{111\}_{\rm fcc}$ family; while for [111] loading, the hcp phase grows into a laminar structure in three planes, which belong to the $\{111\}_{\rm fcc}$ family except for the (111) plane. In addition, the phase transition is evaluated by using the radial distribution functions.

Keywords: single crystal Al, molecular dynamics simulations, uniaxial compression, phase transition

PACS: 64.70.kd, 71.15.Pd, 61.50.Ks, 64.70.K– **DOI:** 10.1088/1674-1056/20/4/046402

1. Introduction

Among the simple metals, aluminum is one of the simplest and most important metal, so it has been the subject of numerous experimental and theoretical studies. On the theoretical side, the phase transition of Al under high pressure has consistently been predicted.[1−4] All of the calculations reported the same phase sequence for Al, fcc–hcp–bcc, but the transition pressures are different. Experiments have also been performed to investigate structural phase transitions in Al.[5−8] Among these studies, reference [7] reported a high pressure experiment up to 219 GPa in fcc Al by using a diamond-anvil-cell, where no structural transformation was found. The phase transition was obtained by Akahama *et al.* using the powder x-ray diffraction method in 2006,[8] where the fcc to hcp transition was confirmed to occur, and the c/a ratios at some constant pressures were analysed in detail. Additional valuable formation from Akahama *et al.*'s experiment is the coexistence of fcc and hcp phases over a wide range of pressures in the transition. However, it is very difficult to apply the direction observation to the structural phase transition in microscopic length, and the corresponding mechanisms are in the absence of experimental information.

Nowadays, molecular dynamics (MD) methods are fruitful in simulating the above complicated phenomena. For example, recently, the mechanism of bcc to hcp transition in iron under compression was successfully investigated at the atomistic level.[9−14] Our previous simulations observed the fcc to hcp transition of Al under uniaxial compression for loading along the [001] direction[15] by MD simulations. However, the lattice orientation with respect to the loading direction has not yet been considered. How the loading direction affects the structural phase transition remains unresolved.

Here, the main purpose of our work is to study how the loading directions influence the structural transition in single crystal Al, and especially the mechanism of structural phase transition. Our simulations show that the structural phase transition is strongly dependent on the crystal orientations. The entire

*Project supported by the Science Foundation for Development of Science and Technology of China Academy of Engineering Physics (Grant Nos. 2008B0101008 and 2009A0101004).

†Corresponding author. E-mail: duan_suqing@iapcm.ac.cn

© 2011 Chinese Physical Society and IOP Publishing Ltd

structural phase transition only occurs when loading along the [001] direction, while for [011] and [111] loadings, only part of the atoms transit to the hcp phase. In addition, the features of the nucleation and propagation of the hcp phase are also different for the three typical orientation loadings.

This paper is organised as follows. In Section 2, we briefly explain the method used in our simulation. In Section 3, we give the results of our simulation and the discussion in detail. Firstly, we discuss the pressure and temperature effects for three direction loadings; then, the morphology evolutions of the structural transition for [011] and [111] loadings are demonstrated and compared, and the corresponding mechanisms are investigated; finally, the radial distribution function (RDF) in the transition is evaluated and used to discuss the phase transition.

2. Methodology of simulation

In our simulation, we adopt the embedded-atom method (EAM) according to Ref. [16] to describe the interatomic force in Al,[16] which has already been widely used for phase transition and deformation researches of the crystal Al.[15,17,18] In order to explore the orientation dependence of structural transition in fcc Al driven by uniaxial compression, we construct three single-crystal Al, samples A, B, and C, to simulate the cases of loading along [001], [011], and [111], respectively. Sample A consists of 256000 atoms, sample B of 250000 atoms, and sample C of 259200 atoms. Periodical boundary conditions are adopted in all three directions. Here, we disregard the effects of boundary condition and the simulation scale. The original temperature in all samples is set at 50 K by the speed calibration method.[19] The initial state is manipulated at zero pressure through modulating lattice constant, and here the lattice constant of the samples are $a = 0.4035$ nm. Loading is implemented by shortening the lattice constants of three orientations step by step along the [001] direction in sample A, [011] direction in sample B, and [111] direction in sample C. The loading rate is $\sim 10^8$, which is in accordance with the rate of laser loading. We use the Verlet algorithm[20] to integrate the equation of motion where the time step is 0.001 ps and the total simulation time is 100 ps. Here, the structure around each atom is resolved by the pair analysis[21] technique. The compressive stress tensor is calculated according to the Virial formula[22]

$$p_{\alpha\beta} = \frac{1}{V}\left(\sum_i m_i v_{i\alpha} v_{i\beta} + \sum_i \sum_{i>j} r_{ij\alpha} f_{ij\beta}\right), \quad (1)$$

where the summation is over all atoms, and $\alpha(\beta)$ represents x, y or z axis. The phase mass fraction analysis is also presented to obtain the phase transition information.

3. Results and discussion

3.1. Pressure and temperature effects

To begin with, we perform the pressure analysis during the loading process. The calculated pressure as a function of compression strain ε is shown in Fig. 1, where $\varepsilon = 1 - V/V_0$ and V_0 is the initial volume of the sample. There are three inflection points, which indicate the beginning of the structural transition in three strain–pressure curves, $P_{\mathrm{s},[001]}$ (0.32, 91 GPa) $P_{\mathrm{s},[011]}$ (0.107, 14 GPa), and $P_{\mathrm{s},[111]}$ (0.114, 17 GPa). From these we can see that the structural transitions are strongly dependent on the crystal orientations. The transition pressure for loading along the [001] direction is about 91 GPa, evidently higher than 14 GPa for [011] loading and 17 GPa for [111] loading. In addition, the pressure–strain curve for [001] loading is lower than the other two curves for [011] and [111] loadings, indicating that samples B and C experience a more evident hardening process than sample A before the transition.

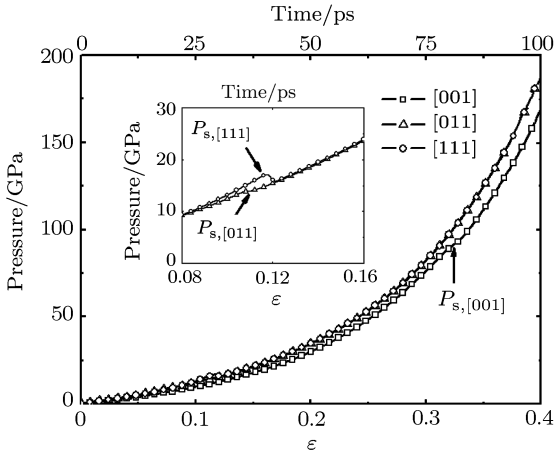


Fig. 1. Pressure versus strain ε and time for loading along the [001], [011], and [111] directions. Points $P_{\mathrm{s},[001]}$(0.32, 91 GPa), $P_{\mathrm{s},[011]}$ (0.107, 14 GPa), and $P_{\mathrm{s},[111]}$ (0.114, 17 GPa) indicate the beginning of structural transition for [001], [011] and [111] loadings, respectively.

The temperature variations with the strain are presented in Fig. 2. With increasing compression strain, the following prominent features can be seen from Fig. 2. (i) The transition temperature is different for the three loadings; it is higher one by one with the sequence of [011], [111] and [001] loadings. Transition starts at about 63.2 K ([011]), 64.5 K ([111]) and

207 K ([001]). Furthermore, the temperature increasing style is different. In samples B and C, the temperatures increase faintly before the structural transition, then alter suddenly at the values of 63.2 K and 64.5 K, respectively. The increasing style of the temperature of sample A is different from samples B and C, as it increases gradually before the phase transition, then increases in an up-stair-manner at 207 K, as can be seen from the labeled points $T_{s,[001]}$ (0.32, 207 K). (ii) The beginning time of transition is different for the three loadings. For the [011] loading, it starts at about 25.4 ps, and for the [111] loading, it starts at about 28.8 ps, while for the [001] loading, it starts at about 80 ps. On the whole, the remarkable distinction in temperature increasing manner and pressure effects in the loading process illustrate that the structural transition features and mechanisms in the three loading directions are different.

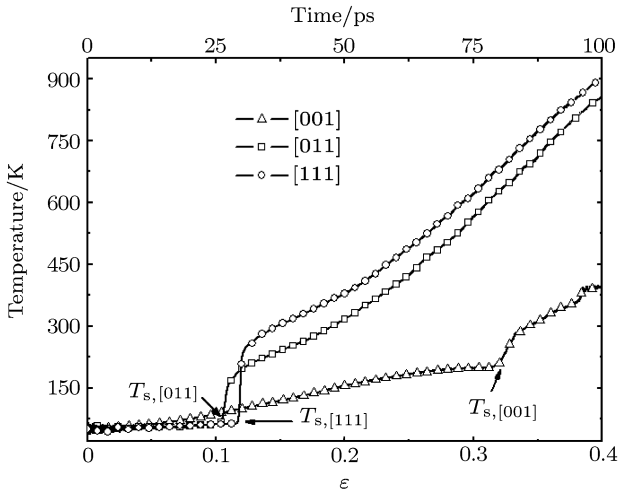


Fig. 2. Temperature as a function of strain ε and time for loading along [001], [011] and [111] directions. Points $T_{s,[001]}$ (0.32, 207 K), $T_{s,[011]}$ (0.107, 63.2 K), and $T_{s,[111]}$ (0.114, 64.5 K) indicate the beginning of structural transition for [001], [011] and [111] loadings, respectively.

3.2. Structural transition features and mechanisms

In order to find out how the hcp phase nucleates and grows, the pair analysis that can distinguish the fcc phase, hcp phase and grain boundaries is used to judge the structural change in a sample.[21] Figure 3 shows the variation in mass fraction λ of the hcp phase with strain ε and time for loading along all three directions. Obviously, about 80% of atoms in sample A turn to form the hcp structure, while in samples B and C, though the mass fraction λ of the hcp phase increases slowly after the critical points of the phase transition, only about 20% of atoms exist in the hcp phase at the end of the loading process. The results mean that the entire phase transition only occurs in the case of loading along the [001] direction. When loading along the [011] and [111] directions, the fcc and hcp phases coexist over a wide range of pressures. The coexistence of the fcc and hcp phases is similar to that reported in Ref. [8]. Similar behaviour has been reported in the pressure-induced fcc–hcp transitions of Xe and Kr.[23] The coexistence between the fcc–Al and hcp–Al phases over a relatively wide pressure region could be attributed to the small total-energy difference between both phases.

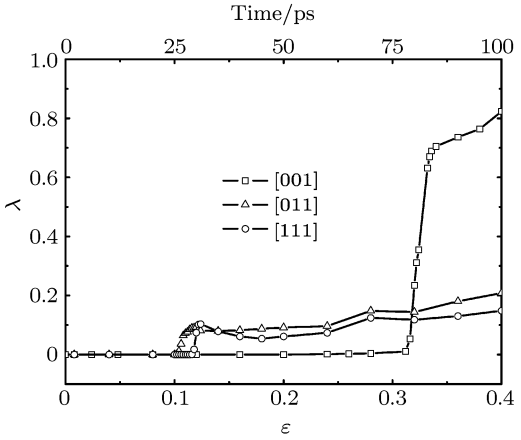


Fig. 3. Variation in mass fractions λ of the hcp phase with strain ε and time for loading along the [001], [011], and [111] directions.

Figure 4 shows the morphology evolution of the structure of sample A. We can see from Fig. 4 that the hcp phase begins nucleating when the strain ε reaches 0.32 (Fig. 4(a)). After the phase transition, the majority of atoms exist in twins in the hcp phase and twin boundaries exist in the (110) plane, residual atoms exist in the fcc stacking faults in the (100) and (010) planes in the end of the loading process (Fig. 4(d)), which was reported in our previous paper.[15] The transformation mechanism for loading along the [001] direction was also described in detail in our previous work, in which it can be realized in a two-step process. In the first step, the fcc (010) plane and (100) plane transit into the hcp (0001) plane. In the second step, the atoms in the area in which the fcc (010) plane transits into the hcp (0001) plane slip along the [100] and $[\bar{1}00]$ directions, and the atoms in the area in which the fcc (100) plane transits into the hcp (0001) plane slip along the [010] and $[0\bar{1}0]$ directions after the sample being contracted (along the [001] direction) to a critical value (about $\varepsilon = 0.32$), and finally results in the hcp phase.[15]

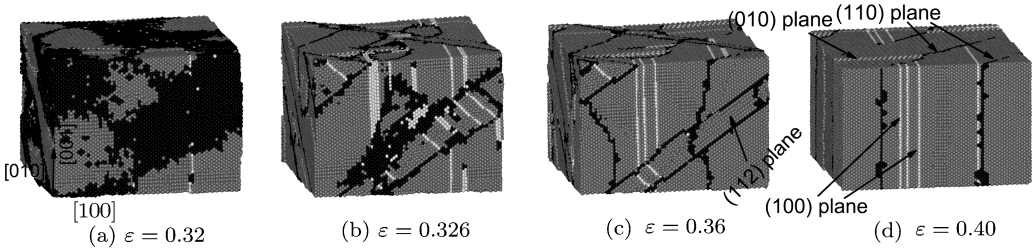


Fig. 4. Morphology evolution of the sample structure in sample A. The compression direction is along the [001] direction. The fcc phase, grain boundaries and hcp phase are shown by the grayish atoms, black atoms and deep gray atoms, respectively. The sample transforms to the hcp structure when the strain oversteps 0.32, and mainly exits in the hcp phase at the end of the loading process.

Figure 5 shows the case of [011] loading. As discussed in the above section, the structural transition features for [011] loading are completely different from [001] loading. One can see from Fig. 3 and Figs. 5(a)–5(h) that only part of atoms (about 20%) transits to the hcp phase. In Fig. 5(a), the partial dislocations begin to appear when the pressure arrives at the $\varepsilon = 0.107$, corresponding to the critical pressure 14 GPa. Then the dislocations move rapidly in four planes ((111), $(\bar{1}11)$, $(1\bar{1}1)$, $(11\bar{1})$) which belong to the $\{111\}_{\rm fcc}$ family, and the area that the dislocation moving forward on $\{111\}_{\rm fcc}$ planes changes from fcc to hcp. It is clear that when the strain reaches 0.136, the hcp phase has grown in the four planes (Figs. 5(b), 5(f)). Subsequently, the hcp phase develops into the typical laminar structure along the four planes, as shown in Figs. 5(c), 5(d), 5(g), and 5(h).

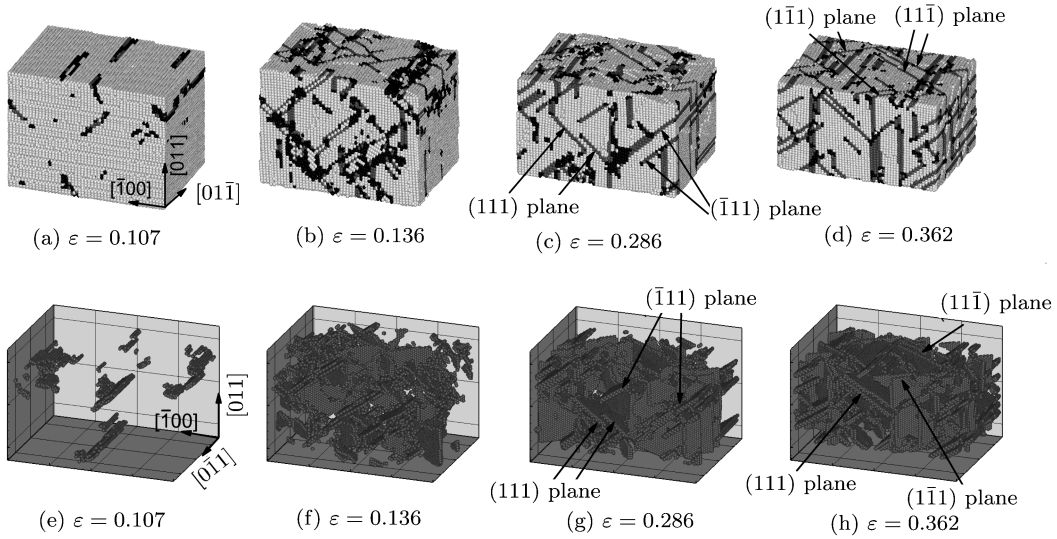


Fig. 5. Morphology evolution of the sample structure 5(a)–5(d) and the hcp phase 5(e)–5(h) in sample B in the loading process. The compression direction is along the [011] direction. The colour criterion is the same as in Fig. 4.

For loading along the [111] direction (Fig. 6), the structural transition features are similar to [011] loading. But because the (111) plane is vertical to the loading direction, the resolved shear stress is zero on the (111) plane in the loading process, so there are no dislocations formed on the (111) plane, which is different from the case of [011] loading. From Figs. 6(a) and 6(e), we can see that when the strain $\varepsilon = 0.118$, corresponding to the critical pressure 17 GPa, the dislocations begin to appear, then they move rapidly on three planes ($(\bar{1}11)$, $(1\bar{1}1)$, $(11\bar{1})$), which belong to the $\{111\}_{\rm fcc}$ family except for the (111) plane (Figs. 6(b), 6(f)). It is clear that the structures in the areas where the dislocations moved forward change from fcc to hcp and form a lot of small flaky structures with increasing compression [Figs. 6(b), 6(f)]. From Fig. 3, a relaxation process right after the critical point $T_{\rm s,[111]}$ has been observed. Although the mass fraction of the hcp phase is reduced, the arrangement of atoms becomes more regular, as shown in Figs. 6(c) and 6(g). At the end of loading, the hcp phase grows to form the typical laminar structure along the three planes ($(\bar{1}11)$, $(1\bar{1}1)$, $(11\bar{1})$), as shown in Figs. 6(d) and 6(h).

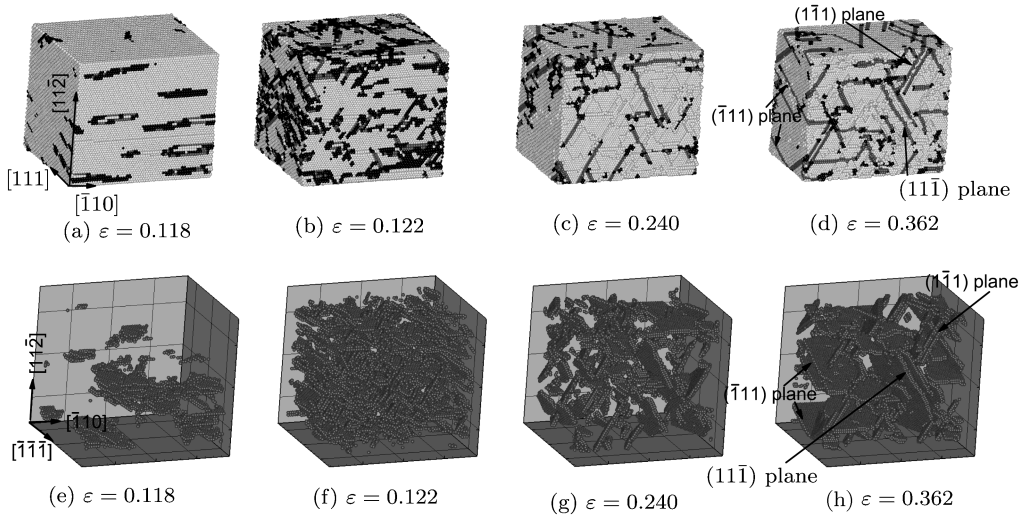
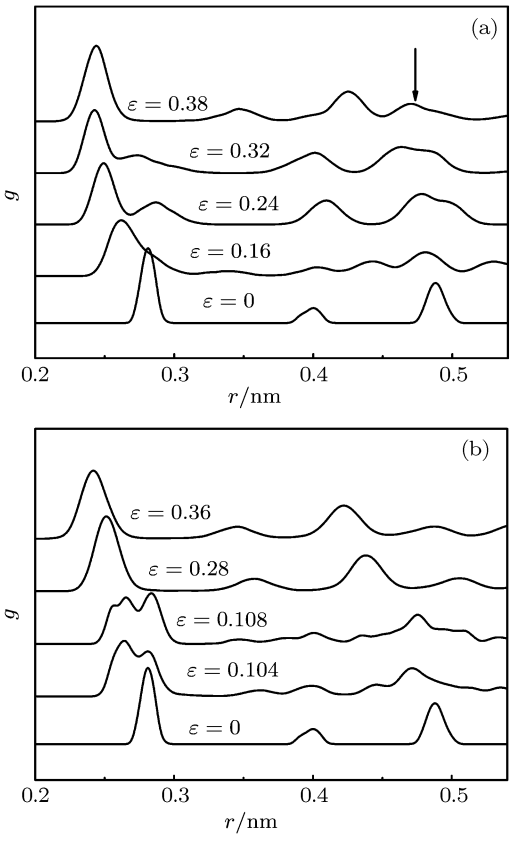


Fig. 6. Morphology evolution of the sample structure 6(a)–6(d) and the hcp phase 6(e)–6(h) in sample C in the loading process. The compression direction is along the [111] direction. The colour criterion is the same as in Fig. 4.

Our simulations indicate that there are different critical pressures for dislocation nucleation and emission in single crystal Al induced by uniaxial loadings. They are 14 GPa and 17 GPa for the [011] and [111] loadings, respectively. When the pressure exceeds the critical value, the dislocations appear in fcc Al and move along the $\{111\}_{\rm fcc}$ planes. The structure changes from fcc to hcp in the areas where the dislocations passed, so the sample partly changes from the fcc to the hcp phase. These results are in agreement with the results of Ref. [24], in which by considering intrinsic stacking fault energies as a function of the pressure, Fanourgakis *et al.* suggested that heavily deformed Al can partially transform to the hcp phase at about 17 GPa by first-principle calculation.[24]

3.3. Radial distribution function analysis

To further clarify the procedure of the fcc to hcp phase transition for the three typical orientation loadings, the radial distribution function (RDF) is evaluated and discussed. Figure 7 displays the RDFs of samples at different strain ε for loading along [001] (a), [011] (b) and [111] (c) directions. Obviously, the curves in Figs. 7(a), 7(b) and 7(c) present initial perfect fcc structures in the range of $r \leq 0.55$ nm when $\varepsilon = 0$, and all peaks in the curves experience an extending process because of the temperature effect. Along with the increase in strain, the first peaks in all three samples deviate towards the left gradually because the lattice constant is compressed continually during the loading process. After the strain reaches 0.104, 0.108 for the [011] loading (Fig. 7(b)) and 0.114, 0.118 for the [111] loading (Fig. 7(c)), the first peaks in the two curves begin to show distinct splitting. In the meantime, some new peaks appear. The distinct splitting of the first peaks and the appearance of new peaks signify the appearance of the new phase, which is brought in by the appearance and movement of dislocations.



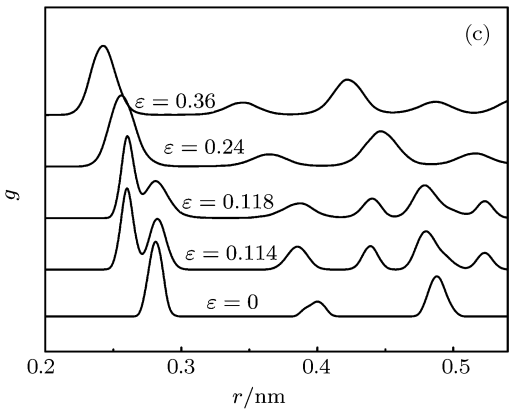


Fig. 7. Radial distribution functions (RDFs) under different strains ε for loading along the [001] (a), [011] (b), and [111] (c) directions.

Otherwise, at the end of loading, the fourth peak, labeled with an arrow in the curve that shows the RDF of sample A at $\varepsilon = 0.38$ in Fig. 7(a), presents the typical hcp phase and is more distinct than that in the RDF curves of sample B and sample C at ε=0.36 in Figs. 7(b) and 7(c). This further illustrates that the hcp phase is the main structure in sample A, while in samples B and C the hcp phase is a subordinate structure after the phase transition.

4. Conclusions

By using the molecular dynamics method, we successfully simulate the process of fcc to hcp structural phase transition in fcc single crystal Al under uniaxial compression along three typical fcc orientations. We find that the transition mechanisms for [011] and [111] loadings are completely different from the [001] loading. For the [001] loading, an entire structural phase transition occurs where the fcc (010) plane or (100) plane transits into the hcp (0001) plane when the pressure preponderates over 91 GPa. For the [011] and [111] loadings, the hcp structure is brought out by the partial dislocations moving along the $\{111\}_{\rm fcc}$ family. There are critical pressures for dislocation nucleation and emission in single crystal Al induced by uniaxial loadings. They are 14 GPa and 17 GPa for the [011] and [111] loadings, respectively. Due to the dissimilar structural phase transition mechanisms, the transition features are completely different for the three loading directions. For [001] loading, the hcp phase exists in twins and twin boundaries along the (110) plane. For the [011] and [111] loadings, only 20% of atoms transit to the hcp structure at the end of the loading process. The hcp phase grows into a laminar structure in four planes ((111), $(\bar{1}11)$, $(1\bar{1}1)$, and $(11\bar{1})$), which all belong to the $\{111\}_{\rm fcc}$ family for [011] loading; while for [111] loading, the hcp phase grows into a laminar structure in three planes, which belong to the $\{111\}_{\rm fcc}$ family except for the (111) plane. The fcc and hcp structures coexist over a wide range of pressures when the pressure is above the critical pressure for the structural transition for [011] and [111] loadings.

References

[1] Moriarty J A and McMahan A K 1981 *Phys. Rev. Lett.* **48** 809
[2] Lam P K and Cohen M L 1983 *Phys. Rev.* B **27** 5986
[3] Boettger J C and Trickey S B 1996 *Phys. Rev.* B **53** 3007
[4] Tambe M J, Bonini N and Marzari N 2008 *Phys. Rev.* B **77** 172102
[5] Loer T, Sigel T, Eidmann K, Foldes I B, Huller S, Massen J, Tsakiris J D, Witkowski S, Preuss W, Nishimura H, Shiraga H, Kato Y, Nakai S and Endo T 1994 *Phys. Rev. Lett.* **72** 3186
[6] Nellis W J, Moriarty J A, Mitchel A C, Ross M, Dandrea R G, Ashcroft N W, Holmes N C and Gathers R G 1988 *Phys. Rev. Lett.* **60** 1414
[7] Green R G, Luo H and Ruoff A L 1994 *Phys. Rev. Lett.* **73** 2075
[8] Akahama Y, Nishimura M, Kinoshita K and Kawamura H 2006 *Phys. Rev. Lett.* **96** 045505
[9] Kadau K, Germann T C, Lomdahl P S and Holian B L 2002 *Science* **296** 1681
[10] Kadau K, Germann T C, Lomdahl P S and Holian B L 2005 *Phys. Rev.* B **72** 064120
[11] Shao J L, Duan S Q, He A M, Qin C S and Wang P 2009 *J. Phys: Comdens. Matter* **21** 245703
[12] Shao J L, Duan S Q, He A M, Qin C S and Wang P 2010 *J. Phys: Comdens. Matter* **22** 355403
[13] Cui X L, Zhu W J, Deng X L, Li Y J and He H L 2006 *Acta Phys. Sin.* **55** 5545 (in Chinese)
[14] Chen Y T, Tang X J and Li Q Z 2010 *Chin. Phys.* B **19** 056402
[15] Li L, Shao J L, Duan S Q and Liang J Q 2010 *New J. Phys.* **12** 033011
[16] Ercolessi F and Adams J B 1994 *Europhys. Lett.* **26** 583
[17] Yamakov V, Wolf D, Phillpot S R, Mukherjee A K and Gleiter H 2002 *Nature Mater.* **1** 45
[18] Yamakov V, Wolf D, Phillpot S R and Gleiter H 2002 *Acta Mater.* **50** 5005
[19] Hoffmann K H 1996 *Computational Physics* (Berlin: Springer) p. 268
[20] Swope W C, Andersen H C, Berens P H and Wilson K R 1982 *J. Chem. Phys.* **76** 637
[21] Honeycutt J D and Andersen H C 1987 *J. Phys. Chem.* **91** 4950
[22] Irving J H and Kirkwood J G 1950 *J. Chem. Phys.* **18** 817
[23] Cynn H, Yoo C S, Baer B, Herbe V L, McMahan A K, Nicol M and Carlson S 2001 *Phys. Rev. Lett.* **86** 4552
[24] Fanourgakis G S, Pontikis V and Ze'rah G 2003 *Phys. Rev.* B **67** 094102